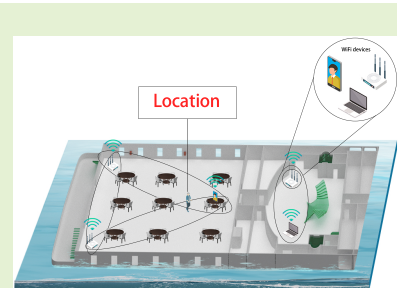


DiFS: WiFi-based Directed Fresnel Signature Localization for Mobile Ship Environment

Kezhong Liu, *member, IEEE*, Guoyu Wang, Cong Chen, Xuming Zeng, Guangmo Tong, and Mozi Chen, *Member, IEEE*,

Abstract— The device-free localization of individuals not equipped with a radio device plays a critical role in cruise ships, particularly during an emergency. In this paper, we introduce a device-free localization scheme requiring low human effort, i.e., DiFS, which utilizes an onboard off-the-shelf WiFi infrastructure. An intuitive idea of DiFS is that because the channel state information (CSI) is sensitive to the target location within the WiFi Fresnel zone, the target location can be determined by extracting the *Fresnel signature* and coordinates of the WiFi access points (APs). However, due to the skin effect of signal propagation onboard a ship, CSI cannot reflect a target with precision. Furthermore, an undirected Fresnel signature may lead to misinterpretation if the WiFi APs are not deployed perfectly. We observed that the power delayed profiles (PDPs) can accurately reflect the target shadowing within the Fresnel zone in a rich multipath environment. In addition, we leverage the specific skin effect in metal ships and infer *directed Fresnel signatures* using a set of power fading models. Extensive experimental results on an actual ship demonstrate that DiFS outperforms the state-of-the-art methods and achieves an accuracy of 0.9 and 1.2 m in the line-of-sight and non-line-of-sight scenarios, respectively.



Index Terms— Device-free indoor localization, Mobile ship environment, Channel State Information (CSI), WiFi

I. INTRODUCTION

INDOOR location-based services have become an essential part of the passenger experience in cruise ships, such as store navigation, elderly care, and emergency navigation [1] [2]. Traditional localization systems are mainly based on additional attached devices, such as mobile phones and radio tags, resulting in limited application scenarios [3]. For example, it is clearly impractical to assume that every passenger onboard carries the proper equipment under such a chaotic and complex scenario as an emergency situation. Missing passengers who have lost their tags may incur tragic consequences during a ship evacuation and rescue procedure [4]. Therefore, localizing a target without relying on any attached devices, dubbed **passive localization**, or a device-free system, has

This work was supported by the National Natural Science Foundation of China (NSFC) under Grant No. 51979216 , Natural Science Foundation of Hubei Province , China, under Grant No. 2021CFA001 and Natural Science Foundation of Hubei Province Youth Program under Grant No. 2022J0059.

K. Liu is with the School of Navigation, Wuhan University of Technology, Wuhan 430063, China, National Engineering Research Center for Water Transport Safety, Wuhan 430063, China and Hubei Key Laboratory of Inland Shipping Technology, Wuhan 430063, China (e-mail: kzliu@whut.edu.cn).

G. Wang is with the School of Navigation, Wuhan University of Technology, Wuhan 430063, China (e-mail:wangguoyu@whut.edu.cn, chenmz@whut.edu.cn, zengxuming@whut.edu.cn).

C. Chen is with the CSSC Cruise Technology Development Co., Ltd., Shanghai 201900, China (e-mail:chenccong@chinacruise.net.cn).

X. Zeng and M. Chen are with the School of Navigation, Wuhan University of Technology, Wuhan 430063, China (e-mail:chenmz@whut.edu.cn, zengxuming@whut.edu.cn).

* Corresponding author: Mozi Chen (chenmz@whut.edu.cn).

emerged as a new research area and has attracted significant attention.

Among all state-of-the-art device-free localization techniques, WiFi-based systems are considered one of the most promising methods owing to their common use on cruise ships and their privacy concerns as compared with video streaming [5] [6] [7]. Furthermore, with the development of open-source WiFi tools, fine-grained channel state information (CSI) can be obtained from commercial off-the-shelf (COTS) WiFi cards, allowing a highly accurate localization when the traditional received signal strength (RSS) is incapable of practical application [3] [8]. CSI-based fingerprint systems have been accordingly proposed owing to their centimeter-level accuracy and adaptability for non-line-of-sight (NLoS) scenarios [9]. However, to achieve such accuracy, laborious site surveys within a ship environment are required for building a comprehensive fingerprint database [10]. Moreover, because radio-frequency signals are sensitive to the environment, any environmental changes, i.e., the moving of furniture or hull deformations caused by ship sailing, will require an exhaustive database update, which is time-consuming and labor-intensive [11] [12]. A **mobile ship environment**, which suffers from inevitable and dynamic hull deformations from internal stress (ship engine and loads) and external sailing conditions (waves and temperature), is impractical for the deployment of a fingerprint-based localization system [13] [14].

In this paper, we propose a WiFi-based Directed Fresnel Signature (DiFS) localization framework for a ship environment. To the best of our knowledge, DiFS is the first system that can passively determine a location in a fingerprint-free

manner using existing WiFi infrastructures present onboard a ship. The intuitive idea is that the Fresnel zones [15] of each WiFi link can form a series of concentric ellipsoidal shapes in the localization space and divide the whole area into multiple subzones. The targets in each subzone can be identified by measuring the WiFi links' status using channel state information (CSI) and compose a unique status sequence, which we refer to as the *Fresnel signature*.

Challenges and our solutions. Although the above basic idea sounds intuitive, there are two main technical challenges: the identification of the precise Fresnel signature and, most importantly, ensuring the **uniqueness** of the Fresnel signature, which makes the DiFS design non-trivial. Specifically, based on our extensive experiments in real-world ships, a consistent pattern change in the CSI of the target within the Fresnel zone does not exist under all indoor ship scenarios due to the complex and rich multipath effects within the metal structure of the ship (see the experiment details in Section III-C.2). To accurately detect onboard targets, we observed that power delay profiles (PDP) can accurately reflect the target's presence compared to raw CSI. Consequently, we proposed a dynamic phase offset sanitization algorithm to remove ship noise from CSI measurements and obtain precise time-domain PDP using Inverse Fast Fourier Transform (IFFT). We then utilize the Rician-K factor to model the shadowing effect of the target on WiFi links and extract the precise Fresnel signature.

Furthermore, DiFS still faces another critical challenge that the Fresnel signature is not unique. Within the framework of the Fresnel zone division, unexpected scenarios exist in which the deployment of WiFi APs will break the uniqueness of the Fresnel signatures, resulting from the inherent undirected nature of the signature, caused by the symmetrical propagation of transceiver links. The undirected Fresnel signatures can significantly degrade the localization accuracy. Facing this challenge, we comprehensively study the specific *skin effect* of the signal propagation caused by metal surface. We observed that the skin effect can be used to break the symmetry of the WiFi propagation scenario and transform the Fresnel signature from an "undirected" to a "directed" signature. Based on this observation, we proposed a "skin" wave identification method by using a set of power fading models to efficiently estimate the direction of the target in Fresnel zone and hold the uniqueness of the Fresnel signature.

Finally, based on the directed Fresnel signature, we design the localization scheme by constructing a complete Fresnel signature table of the localization space, and we further expand the system from a single- to multiple-target localization to enhance the efficiency of the DiFS. We implement a prototype DiFS and deployed onboard an actual passenger ship. Extensive experiment results show that DiFS outperforms the state-of-the-art methods and achieves an accuracy of 0.9 and 1.2 m in line-of-sight and non-line-of-sight scenarios, respectively.

The contributions of this study are as follows:

- We propose a way to detect a target within the Fresnel zone of the WiFi links in a ship environment with insight from the PDP, which conveys comprehensive shadowing information under a rich multipath scenario.
- We define and propose a directed Fresnel signature and

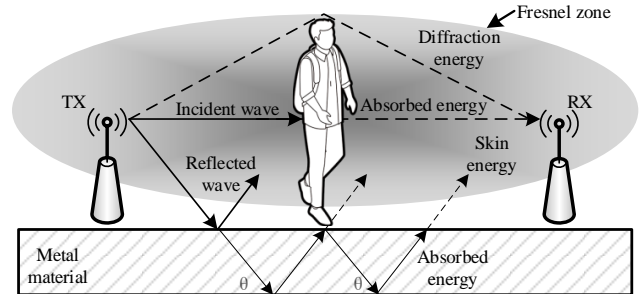


Fig. 1: Wireless signal propagation in a metal environment.

validate its effective estimation of the target direction in the Fresnel zone based on a unique skin effect caused by a metal structure.

- We extend our design to multiple target localizations and implement the DiFS system in a mobile ship environment with commercial WiFi devices.

II. MOTIVATIONS

While there has been an amount of WiFi-based fingerprint-free indoor localization techniques, in this section, we motivate our study by presenting the unique character of the **mobile ship environment**, and discussing how the special environment affect the existing systems.

A. Metal Structure

Among recent WiFi-based indoor localization techniques, most works are concentrated on the general environment, i.e. office and house. Fig. 1 shows a typical WiFi localization system, which consists of three parts: a signal transmitter (Tx), a signal receiver (Rx) and the localizing target that blocks the WiFi signal. Typically, the location of the target can be estimated using the CSI collected at Tx combined with the signal power fading model [3]. However, wireless propagation onboard a ship tends to be less regular because the geometric and dielectric characteristics change dramatically in metal-structured cabins [16]. As for the 2.4 GHz WiFi signals, the partition loss of the transmitted power can reach up to 40 dBm, whereas most of the radio waves are reflected by the metal surface. The dielectric property of a metal surface can lead to a large number of reflected waves and significantly increase the multipath effect at the end of the receivers. In addition, the **skin effect** is another influencing factor on wireless propagation. According to the wireless propagation, when the radio waves encounter a conductor, i.e., a metal wall, the waves tend to become distributed on the surface owing to opposing eddy currents induced by the changing magnetic field [17]. The magnetic field intensity is largest near the surface and decreases with the depths along the wall. In other words, the radio waves can flow at the "skin" of the wall and induce more transmitted radio paths in the environment, which increases the multipath effect as shown in Fig. 1.

Such a unique multipath-rich environment would bring huge noise on the phase and received signal power (i.e. RSS) measurements in commercial WiFi devices [18]. Specifically,

the range d between a pair of Tx and Rx can be estimated using signal power by

$$d = 10^{-\frac{P_r}{40}} \cdot \lambda \cdot \frac{\sqrt{G_t \cdot G_r \cdot P_t}}{4\pi\gamma} \quad (1)$$

where P_r is the RSS measurements in dB, P_t is the RSS of transmitter, λ is the WiFi wavelength, γ is the environmental factor, G_r and G_t are the gain factor of the receiver and transmitter antenna gain factor, respectively. Based on this equation, we can obtain the distance estimation error e_d defined as

$$e_d = |1 - \frac{d_e}{d_t}| = |1 - 10^{-\frac{P_e - P_t}{40}}| \quad (2)$$

where d_e and d_t are estimated range in noisy ship environment and its true value, P_e and P_t are estimated RSS in noisy ship environment and its true value, respectively. That is to say, the distance error for the 2 dB or 10 dB RSS noise level would be -1.1 m or -4.4 m, respectively. According to the previous work [11] [12] [19] [20], the distance estimation error in ship exceeds the decimeter-level accuracy requirement for most localization-based services.

B. Mobile Environment

Apart from a rich multipath effect in a metal structure environment, a phase shift, here we called **dynamic phase offset (DPO)**, also occurs between every WiFi Tx-Rx pair owing to the dynamic change of the mobile ship. Unlike a static indoor environment (e.g., land buildings), ships are built using engines for powering through seawater under various sailing conditions. When voyaging, the ship's hull is subject to inevitable deformations, including static angular deformation and dynamic angular deformation, caused by the external stress of loads, waves, and external temperature changes [13]. Owing to these deformations of the sailing ship, the equipment position deployed indoors (e.g. radar antennas and WiFi antennas) may differ significantly from the original setup parameters. As a result, this dynamic deformation changes the time-of-flight (ToF) from packet to packet for the same Tx-Rx pair, and in turn results in additive noise in the phase estimates across the packets, which we call DPO of the CSI as shown in Fig. 2.

Based on our observation, the ship deformation caused by ship sailing can significantly change the wireless signal propagation paths. The ship static angular deformations can amount to 1° due to the redistribution of freight and fuel. The non-uniform heating of different ship parts under the sun also may lead to up to 1° change. As for the dynamic angular deformations, they are caused by hull motion, wave impact, helm steering, and can be as high as 1° - 1.5° [16] [14]. Specifically, consider a M -element antenna array as shown in Fig 2. The signal path angle-of-arrived (AoA) θ can be estimated by

$$\theta = \arccos(\lambda \cdot \frac{|\phi_i - \phi_j|}{4\pi D_{i,j}}) \quad (3)$$

where ϕ_i and ϕ_j represent the received phase of the i -th and j -th antenna. $D_{i,j}$ denotes the dynamic distance between two

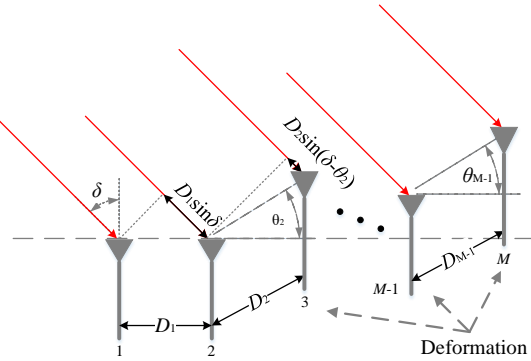


Fig. 2: Signal phase shift caused by the deformed ship hull in a mobile environment.

antennas caused by hull deformation. λ is the wavelength. As can be seen, the deformation can cause offsets θ_i on the phase measurements. And according to Eq. 3, even a 0.5 radians phase noise can result in an AoA error of 9 - 32° . WiFi-based indoor localization techniques mostly rely on exploring the slight difference of signal propagation paths introduced by the existence of the people. Thus, these methods are vulnerable in the mobile environment such as ships, where the subtle environmental changes may confuse the CSI measurements.

C. Performance of Existing Techniques

In this part, we motivate our study by presenting the performance of state-of-the-art WiFi-based indoor localization techniques using in the mobile ship environment. Although there has been an increase in the exploration of WiFi for passive localization in recent years, studies for mobile ship environment is relatively rare. The strategies for general environment WiFi-based passive localization can be divided into two categories, namely, model-based and fingerprint-based localization. As physical model-based methods, LiFS [3] leveraged the shadowing effect of targets near the line-of-sight of the links and an accurate power fading model to estimate the location. SpotFi [21] utilizes the phase difference between the antenna array and estimates the AoA of the LoS path of the target. Widar2.0 [5] proposed a CSI-motion model to jointly estimate the Doppler frequency shift (DFS), AoA and ToF and achieve a target tracking. As fingerprint-based methods, Pilot [7] utilized a Wi-Fi CSI as a fingerprint to localize an individual in one of the fingerprinted locations. SWIM [19] explored and quantized the influence of a mobile ship and constructed a 3D fingerprint map for indoor ship localization. AutoFi [22] proposed an auto-calibration approach to collect the CSI of a non-human environment after environment layout changes and predict the fingerprint variations. However, the above techniques all exist shortcomings of being deployed in the ship. Through our previous experiments conducted on a real-world cruise ship [20], the model-based localization systems are facing a huge accuracy degradation when the ship sets sailing. Either based on AoA, fingerprint or attenuation model, all suffer from ship sailing-induced impacts. On the other hand, the methods designed for a dynamic environment,

TABLE I: A comparison of state-of-the-art works for passive WiFi-based localization in ship environment

Properties	LiFS	Widar2.0	SpotFi	Pilot	SWIM	AutoFi	DiFS
Localization Type	Passive	Passive	Active	Passive	Passive	Passive	Passive
Method	Attenuation	ToF/AoA	AoA	Fingerprint	Fingerprint	Fingerprint	Fresnel signature
# (Tx, Rx)	(4, 7)	(1, 1)	(4, 2)	(2, 2)	(1, 1)	(1, 1)	(4, 5)
Scenario	Static	Static	Static	Dynamic	Dynamic	Dynamic	Dynamic
Track static object	Yes	No	Yes	Yes	Yes	Yes	Yes
Range	12 m	8 m	8 m	11 m	8 m	7 m	12 m
Accuracy on the ground	0.72 m	0.75 m	0.51 m	0.53 m	0.53 m	0.53 m	1.24 m
Accuracy in Ship	2.82 m	-	2.04 m	1.77 m	1.22 m	1.47 m	1.24 m

i.e. SWIM and AutoFi request huge human efforts to calibrate the radio map. The techniques are as shown in Table. I.

III. METHODOLOGY OF DIFS

To overcome the above issues, in this part, we propose our solution DiFS. Before we describe each step of the design in detail, in this section, we first mention the concept of DiFS along with its three basic ideas, i.e., a Fresnel zone, WiFi CSI, and Fresnel signature, and illustrate them through some examples.

A. Fresnel Zone Detection with CSI

In general indoor environments, wireless signals can transmit from a transmitter to a receiver through multiple paths, i.e., line-of-sight (LoS) and NLoS paths. NLoS paths include reflections, scattering, and diffraction paths. The appearance of individuals between a paired transmitter and receiver tends to significantly change the signal paths, which leads to a sophisticated signal composition at the receiver, which is referred to as a multipath effect [23].

In the absence of individuals, we assume that a total of n reflection paths are received by the receiver. Since the positions of the transmitter and receiver are fixed, based on the WiFi signal's attenuation characteristics, we can determine the signal transmission distance. Using this information, we construct n concentric ellipses as depicted in Fig. 3a. When a subject under test enters the area, the absorption and obstruction of the WiFi signal by the human body lead to a reduction in the power of the corresponding reflection paths or Line-of-Sight (LoS) paths. As a result, we can ascertain whether the target is within the test area and further identify between which two concentric ellipses the target is located. A signal propagation region can be characterized by a series of concentric ellipsoidal zones along the transmitter-receiver (Tx-Rx) link, which is known as a **Fresnel zone** [24]. The radius of the circular cross section of a Fresnel zone is given as follows:

$$|P_T Q_n| + |Q_n P_R| = |P_T P_R| + n\lambda/2 \quad (4)$$

where Q_n is the trajectory of the ellipse at the n -th Fresnel zone and λ is the wavelength of the wireless signal. In other words, within the Fresnel zone, a human object diffracts and reflects the signal wave paths, resulting in constructive or destructive interference of the wave strength that can be detected. According to wireless communication principles, the

sensitivity of the receiver increases from the outer Fresnel zone to the inner Fresnel zone. With a larger zone, the receiver becomes insensitive.

Most modern digital radio systems use an OFDM framework to transmit signals at different frequencies through orthogonal subcarriers. The CSI is fine-grain physical layer information that describes the properties of a communication link at each subcarrier based on the channel frequency response (CFR). The transmitted symbol $X(f)$ within the frequency domain is modulated on a subcarrier frequency f , and the received symbol $Y(f)$ depends on the CFR $H(f)$:

$$Y(f) = H(f) \times X(f) \quad (5)$$

The CSI is a sample version of the CFR and depicts the amplitude and phase of a subcarrier. The CSI measurements can be obtained by leveraging commercial WiFi network interface cards (NICs), such as an Intel 5300 and an Atheros 9390, with public open-source tools [25] [26]. With WiFi 802.11n/g, the physical layer allocates the spectrum resources (20 MHz bandwidth) of the 2.4 GHz band to 64 orthogonal subcarriers, where the frequency spacing between any two neighboring subcarriers is 0.3125 MHz. The CSI tools utilize a channel sounding mechanism in WiFi 802.11n/g to report the CSI from the receiver for every received frame and send it to the software driver. Each channel matrix entry is a complex number, with a signed 8-bit resolution for both the real and imaginary parts, and can be converted into the following:

$$H(f_i) = |H(f_i)| e^{j \sin(\angle H(f_i))} \quad (6)$$

where f_i is the central frequency of the subcarriers ($i = 1, \dots, M$), $|H(f_i)|$ denotes its amplitude, and $\angle H(f_i)$ denotes the phase. The gain and phase of the spatial path between a single pair of transmit-receive antennas are also specified.

That is, the CSI measures the power fading of the WiFi link between the transmitter and receiver, which can be used to detect and measure the Fresnel zone, as shown in Fig. 3. Among them, Fig. 3b illustrates that the CSI amplitudes of all sub-carriers are decreased when a target is located within the Fresnel zone in an outdoor space, and Fig. 3c shows that there are parts of the subcarriers that can accurately reflect the transition of the target's location change, although not all subcarriers are feasible owing to the multipath effect in an indoor space [27].

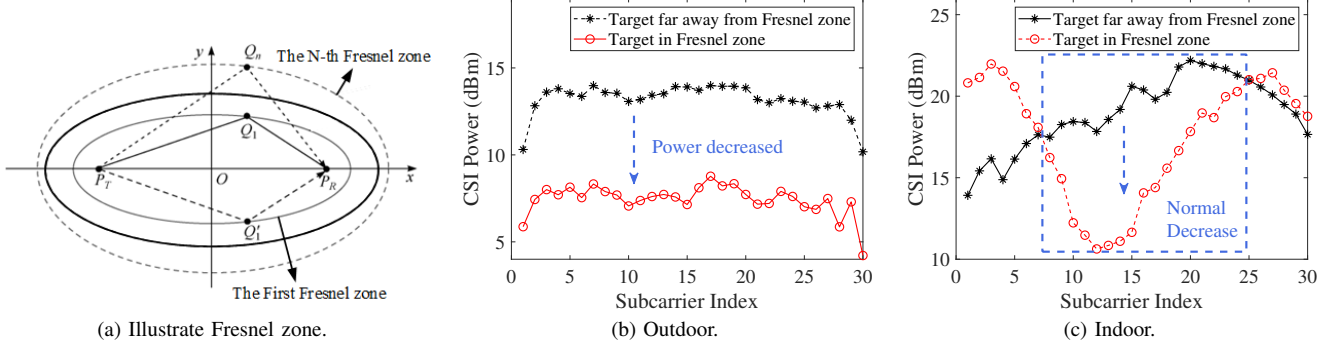


Fig. 3: CSI measurements with a target inside and outside of the Fresnel zone in outdoor and indoor environments.

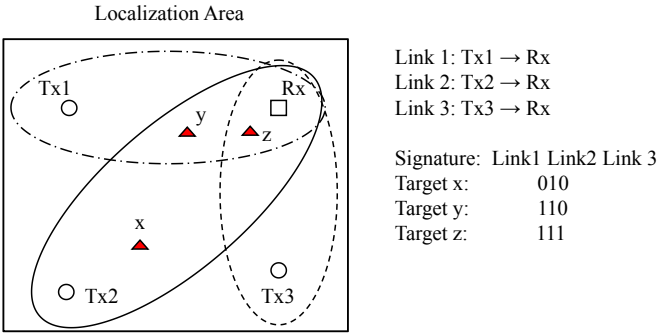


Fig. 4: An example of Fresnel zone division with three links.

B. Fresnel Signature

In this part, we define the Fresnel signature and illustrate it through an example. Assume that a 2D localization space (the most common scenario) consists of n pairs of transmitter-receiver links. The links can be modeled as an ellipse (an ellipsoid in a 3D scenario) according to the Fresnel theory. For one ellipse, the localization area can be divided into two different subzones that can be distinguished based on the CSI of the communication links, as introduced above. Similarly, an ellipse can be drawn for all n links, and the localization space can be divided into numerous subzones, as illustrated in Fig. 4. For each subzone created by the Fresnel ellipses induced by the transmitter-receiver pairs, the CSI amplitude will behave differently when a human target is localized within it from the perspective of all communication link qualities. A signature $s = (I_{link1}, I_{link2}, I_{link3})$ consisting of a sequence of CSI amplitude indications with an index of the link order can be used to immediately determine the location of a target without any other costs incurred.

Definition 1. A **subzone** is the set of points whose members own the same signature in the Fresnel zone segmentation.

For example, as shown in Fig. 4, the signature at positions x , y , and z will be $s_x = 010$, $s_y = 110$, and $s_z = 111$, respectively, where 1 indicates the detection of a power degradation of the link, and vice versa. The signatures can be consistent as long as the location of the transmitters and receivers is fixed. We call this ordered sequence of Fresnel

link indications a **Fresnel signature**.

Theorem 1. Let L be the set of WiFi links, and the numbers of subzones induced by M transmitters and N receivers are then $(M \cdot N)^2 - M \cdot N + 2$ at most.

Proof: Suppose there are M APs, N clients, and one target, which are randomly located in a 2D monitoring area. The number of wireless links between APs and clients is $M \cdot N$. Thus, based on the previously introduced Fresnel zone model, we can establish a number of $L = M \cdot N$ ellipses to restrict the location of the target. For every additional link, these L ellipses intersect by $\text{part}(L) = \text{part}(L-1) + 2*(L-1)$ at most. Therefore, the maximum number of unique Fresnel signatures is $(M \cdot N)^2 - M \cdot N + 2$.

Using the CSI amplitude degradation and thus the corresponding Fresnel signatures, we can achieve human localization in a fingerprinting-free and passive way. However, some practical challenges still exist when used in a ship environment.

C. Practical Issues

Although Fresnel zone division (FZD) localization can avoid laborious human effort and high infrastructure costs that occur in most device-free designs, challenges still remain. In this section, we describe three practical challenges encountered when deployed in a mobile ship environment, including an undirected Fresnel signature, the skin effect, and dynamic phase shift, in the DIFS.

1) Undirected Fresnel Signature: Although the FZD has a lower overhead and is relatively accurate, some unexpected and vicious scenarios can break the uniqueness of the signatures. A distracting scenario, as shown in Fig. 5, can be created from the deployment of WiFi APs (which are usually unmovable aboard a cruise ships). Within this 2D localization area, the targets x and y are both in and out of the Fresnel zone of Links 1 and 2, with target x close to the receiver of the link, and target y close to the transmitter. In the middle area, target z is within the interaction region of the Fresnel zone of the two links. Under these circumstances, the vicious deployment of two transmitter-receiver pairs results in misleading signatures, as shown in the figure. The signature of z is 11, whereas the signatures of x and y are both 01. Based on the FZD calculation, these three targets share a similar

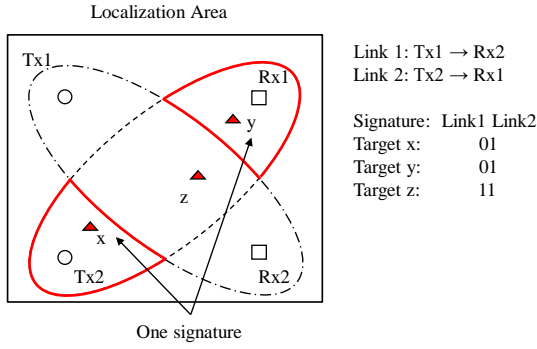


Fig. 5: An example of undirected Fresnel signatures.

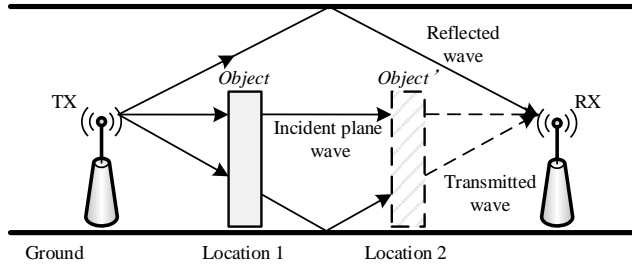


Fig. 6: Symmetry in Fresnel zone.

location result if we use the centroid of the subzone. These misleading signatures can significantly reduce the localization accuracy of the FZD technique. That is, when the target moves along the LoS path from the transmitter to the receiver, the CSI measurements change symmetrically, making it difficult to identify which of the axially symmetric or centrally symmetric regions the target is located in. This is called an "undirected signature".

This issue formed our motivation to search for a solution to a directed Fresnel signature. However, it is nearly impossible to determine the relational distance of the target between the receiver and transmitter owing to the symmetry of the environment, as shown in Fig. 6. According to the reciprocity theorem of WiFi propagation, if the distance from the target to the receiver or transmitter is equal, the signals received by the receiver will remain the same regardless of which target the receiver is closest to. When a target moves along

the LoS path from the transmitter to the receiver, the CSI measurements have a symmetrical variation. (The raw data from the experiment are provided in Section IV-C.)

2) WiFi CSI in Metallic Ship: Targets in the Fresnel zone can be detected using the CSI amplitude with high accuracy in both outdoor and general indoor environments, as described in Section III-A. However, the efficiency in a ship environment remains uncertain.

To evaluate the performance in such a ship environment, we conducted experiments onboard an actual inland cruise ship, namely, China Goddess 2 Cruise. Two typical scenes were evaluated, i.e., a dining room of $15m \times 20m$, and a hall of $7.5m \times 13.5m$. Details on the experiment devices can be found in Section V-B. The distance between the transmitter and receiver is 6 m at the same height, as shown in Fig 7. In each scene, we collected two sets of CSI measurements when a target is inside and outside the Fresnel zone, the results of which are shown in Fig. 8. As can be seen, the pattern of the changes in CSI amplitude are different in each ship scene. In a corridor, the power of half of the subcarriers (from indexes 16 to 29) decreases when the target is located in the Fresnel zone, and that of the other half increases. The CSI measurements in the dining room and hall are completely opposite when the target is in the Fresnel zone. As a result, the CSI amplitude-based Fresnel detection cannot be directly applied in such a metal environment.

3) WiFi Phase in Dynamic Environment: The FZD is used to explore the slight difference in signal propagation, reflection, and absorption by humans within the Fresnel zone. The DPO brings about an unacceptable phase error when measuring the wireless channel and degrades the FZD performance in such a dynamic and inconsistent environment.

IV. DESIGN OF DiFS

In this section, specific solutions for the tasks mentioned in the last section are discussed, including the precise power delay acquirement, PDP-based Fresnel detection, directed Fresnel identification, and localization of the DiFS system.

A. Precise Power Delay Acquirement

Because the amplitude of the Wi-Fi subcarriers, which describes the signal propagation from the frequency domain, fails to recognize people within the Fresnel zone owing to complex multipath effects in a ship environment, as described in Section III-C.2, in this section, we also propose transforming the CSI into the time domain, and seek an accurate Fresnel zone detection method that can be used onboard a ship. Theoretically, the frequency-domain CSI can be transformed into a lossless time domain **power delay profile (PDP)** through an IFFT. The PDP describes the power strength of a received signal as a function of the arrival delay and explicitly profile the multipath propagation of the signal within the environment. However, to obtain a precise PDP, accurate CSI phase measurements require to estimate the real time-of-flight of the signal. In this paper, we used Intel 5300 wireless NICs as transceivers. The receiver was equipped with 3 receiving antennas, and the WiFi signal contained 30 subcarrier groups,

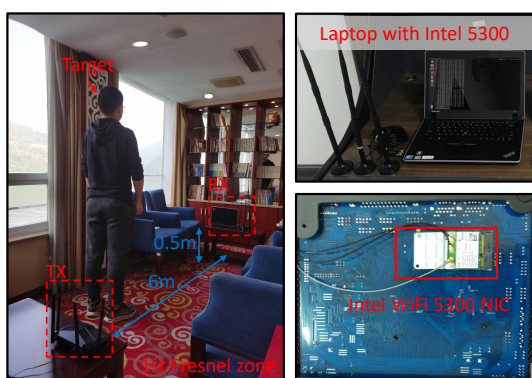


Fig. 7: Experiment scenes in passenger ship.

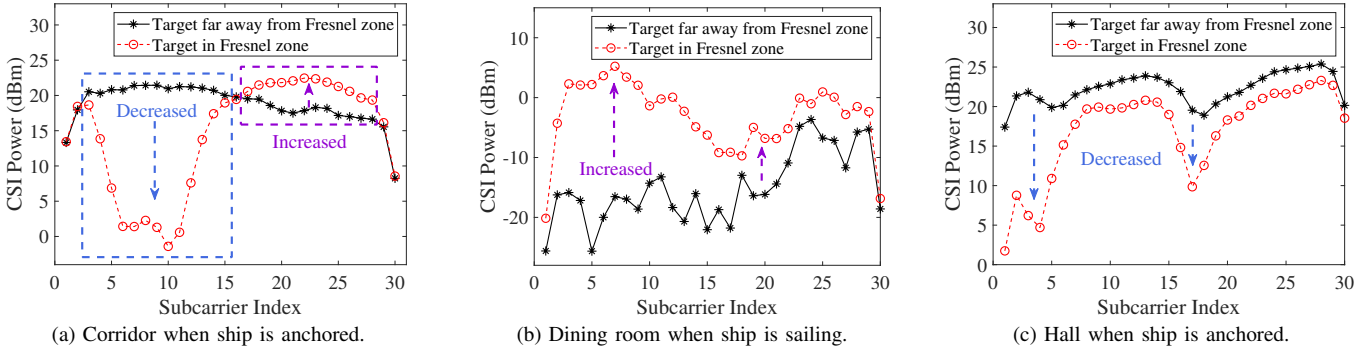


Fig. 8: CSI amplitudes of all subcarriers when the target is inside/outside of the Fresnel zone under three different scenarios.

$$\begin{bmatrix} CSI_{1,1} & \dots & CSI_{1,16} & CSI_{2,1} & CSI_{2,16} \\ \dots & \dots & \dots & \dots & \dots \\ CSI_{1,15} & \dots & CSI_{1,30} & CSI_{2,15} & CSI_{2,30} \\ CSI_{2,1} & \dots & CSI_{2,16} & CSI_{3,1} & CSI_{3,16} \\ \dots & \dots & \dots & \dots & \dots \\ CSI_{2,15} & \dots & CSI_{2,30} & CSI_{3,15} & CSI_{3,30} \end{bmatrix}$$

Fig. 9: Illustration of the CSI matrix after CSI smoothing.

which is approximately one group for every two subcarriers at 20 MHz. We obtained a 3x30 CSI matrix. However, since this CSI matrix does not sufficiently represent all reflection paths in the ship environment, we expanded it to a 30x30 matrix through CSI smoothing. CSI smoothing was initially proposed in [21] to identify more multipath signals in the case of having only 3 antennas. This method leverages the phase shift between corresponding elements of the two sensor subarrays is connected through a common scaling factor, we extend the CSI matrix to a 30*30 matrix by smoothing its elements. The results are shown as Fig 9.

The CSI phase is contaminated owing to the DPO, as described in Section IV. Such a slight phase error will result in a significant inaccuracy in deriving the PDP owing to the decrease in the phase value within a small range of $(-\pi, \pi)$. In this part, we propose a way to obtain a precise phase in a commercial WiFi card in a ship environment. An experiment dataset was collected onboard a sailing ship, and the unwrapped CSI phase is as shown in Fig. 10a. As can be seen, although the CSI phase variation between the two packets is significant and the added phase owing to the DPO differs for the CSI observed at two antennas, the phase shift between different packets incurs a constant offset from the phase estimates of all subcarriers. This additional dynamic delay manifests itself linearly within the frequency term in the phase of all channels. Hence, a DPO of $\phi_s = -2\pi f_\delta(n-1)\tau_s$ results in adding to the phase of the CSI value of the n -th subcarrier, where $\tau_s = d_s/C$ is the signal flight time offset caused by a dynamic ship hull deformation d_s . Based on this observation, we propose a dynamic phase sanitization algorithm using the linear fitting method described

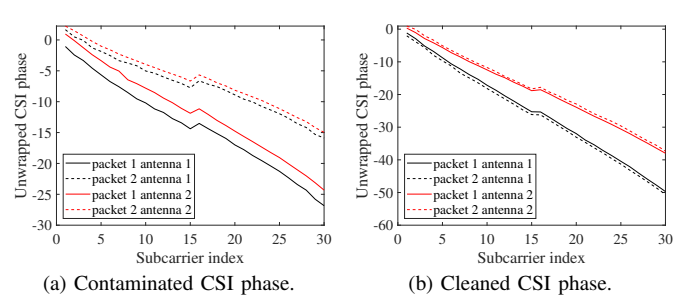


Fig. 10: Contaminated and cleaned CSI phases.

in Algorithm 1.

Claim1: *The proposed dynamic phase sanitation scheme removes the DPO and preserves the relatively accurate CSI phase measurements.*

Let us consider two consecutive packets transmitted by the target. Let $\theta_i(m, n)$ represent the unwrapped phase response of the channel for the i -th packet at n -th subcarrier of m -th antenna, and $\phi_{m,n,i}$ be the DPO for the i -th packet of the same subcarrier and antenna. By applying the phase sanitization algorithm, we can remove the linear fit of the CSI phase response for the first packet to obtain a modified phase response $\hat{\theta}_1(m, n)$. For example, we can obtain a modified CSI phase of the second packet $\hat{\theta}_2$ by $\hat{\theta}_2 = \theta_2(m, n) - 2\pi f_\delta(n-1)d_{s,1}/C$ and the phase $d_{s,1}$ of the first packet. The actual and modified CSI phase responses for two packets obtained from the CSI collected from our experiments are shown in Figure 10b. The cleaned CSI phase, obtained by applying Algorithm 1, is then free from the DPO. The cleaned CSI can then be obtained by removing the dynamic DPO of the unwrapped phase collected from all of the antennas. With IFFT processing of the cleaned CSI, we can obtain the PDP within the time domain, i.e., $p(t)$.

B. PDP-based Fresnel Detection

After obtaining the precise PDP from commercial WiFi NICs, in this part, we propose a PDP-based Fresnel detection method that can overcome the complex multipath effect onboard a ship and accurately detect people within the Fresnel zone.

Claim2: *The PDP transformed from a processed CSI is*

Algorithm 1 Dynamic phase sanitization algorithm.

Input: A CSI sequence, $H = \{H_i\}$, and unwrapped CSI phase θ_i for the i -th packet;

Output: The sanitized CSI phase $\hat{\theta}_i$;

- 1: Obtain the best linear fit of the unwrapped CSI phase as follows:

$$\hat{d}_{s,i} = \arg \min_{d_s} \sum_{m,n=1}^{M,N} (\theta_i(m,n) + 2\pi f_\delta(n-1)d_s/C + \beta)^2; \quad (7)$$

- 2: From the unwrapped CSI phase, subtract the phase that would have been added owing to a dynamic phase shift:

$$\hat{\theta}_i(m,n) = \theta_i(m,n) - 2\pi f_\delta(n-1)\hat{d}_{s,i}/C \quad (8)$$

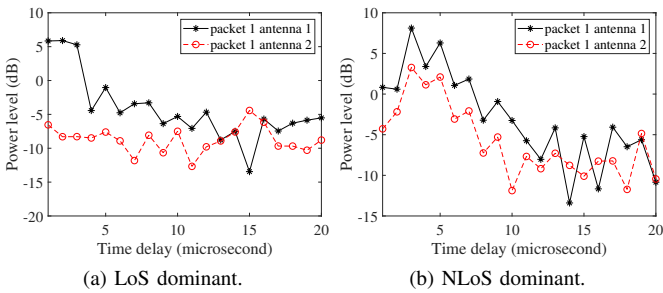


Fig. 11: Identifying LoS scenario using PDP.

a fine-grained time-domain indicator of the target within the Fresnel zone.

As previously described, a PDP can directly represent multipath signals with different arrival times within the time domain. As shown in Figure 11, we present the PDP obtained under scenarios of both the LoS and the presence of people within the Fresnel zone, which we denote herein as NLoS. As can be seen, the two PDPs in Figure 11a from two antennas indicate the existence of the LoS path between the first multipath components that have the strongest power strength. By contrast, the first arriving signal in Figure 11b is weaker than the later arriving signals, which indicates that an obstacle is present in the LoS path.

1) **Rician-K Factor:** Although we seem to be able to easily distinguish the existence of people within the Fresnel zone using the above PDP characteristic, in practice, owing to the noisy readings of conventional signal strength indicators in the hardware and MAC layer, such a method generally stops working during the simulation or is only partially completed in an outdoor environment. In a real-world ship experiment, the path with the smallest time delay may not be the LoS path because a direct path may be too weak compared to the NLoS paths reflected by the walls or other objects occurring under numerous indoor scenarios. In addition, owing to the non-synchronized clocks of commercial Wi-Fi transmitters, the assumption that the path with the lowest time-of-flight (ToF) is the direct path is a mistake. Focusing on this problem, we propose an accurate Fresnel detection algorithm for DiFS that utilizes an envelope distribution-based scheme to explore the

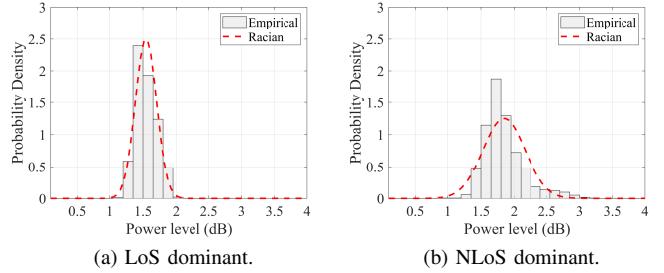


Fig. 12: Distribution of the first arriving signal power.

spatial domain of the Fresnel zone.

The **intuition** here is that people within the Fresnel zone often involve large numbers of reflection, refraction, and diffraction signal paths, leading to more random NLoS paths, as shown in Fig. 1. By comparing the distributions of the first arriving power envelope, a LoS dominant condition and the existence of the target can be identified and distinguished. Herein, we use a Rician envelope distribution to model the LoS-dominant condition. In this case, $h[l]$, for one path of l , can be modeled as follows:

$$h(l) = \sqrt{\frac{K}{K+1}} \sigma_l e^{j\theta} + \sqrt{\frac{1}{K+1}} \mathcal{CN}(\mu, \sigma^2), \quad (9)$$

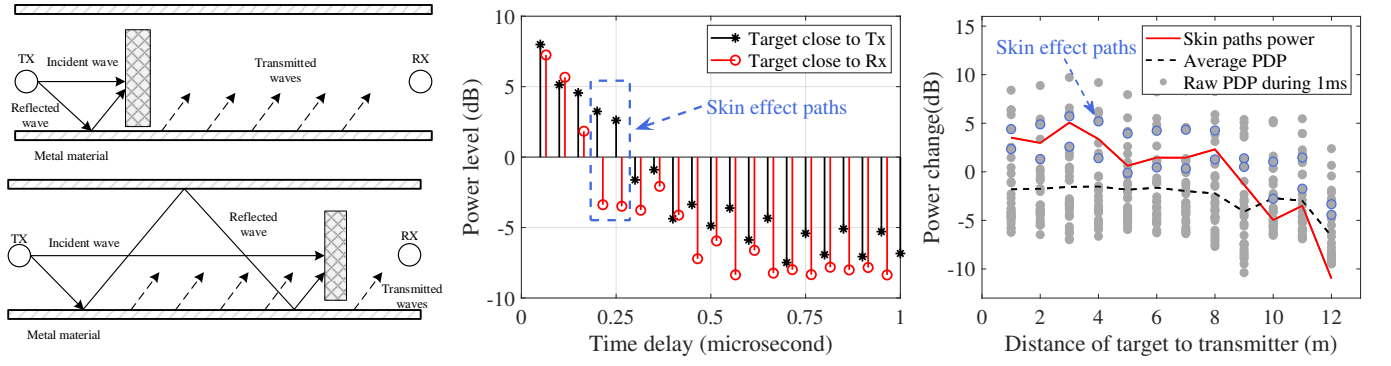
using the first term corresponding to the LoS path arriving with a uniform phase θ and the second term corresponding to the aggregation of the large number of reflected and scattered paths, independent of θ . The goal is to measure the envelope distribution of a filtered CSI for a link and compare it with a theoretical Rician distribution if no actual distribution exists. However, it often requires large numbers of measurements to obtain an accurate probability density estimation, which limits its real-time applicability. Toward a lightweight yet effective feature, we utilize the Rician- K factor for our Fresnel detection. The Rician- K factor [28] (also called the K -factor) is the ratio of power in the LoS component to the power in the scattered NLoS paths and can be obtained as follows:

$$\hat{K} = \frac{-2\hat{\mu}_2^2 + \hat{\mu}_4 - \hat{\mu}_2\sqrt{2\hat{\mu}_2^2 - \hat{\mu}_4}}{\hat{\mu}_2^2 - \hat{\mu}_4}, \quad (10)$$

where $\hat{\mu}_2$ and $\hat{\mu}_4$ are the empirical 2nd and 4th order moments of the measured data, respectively. A larger K indicates a more deterministic nature of a LoS path channel and thus less probability of people being present within the Fresnel zone.

2) **Fresnel Detection:** To further overcome the non-synchronized clock problem of a WiFi device and extract the precise first arriving signal power from the PDP samples, we propose a pre-processing scheme as follows:

- First, we normalize the samples by dividing them with the average amplitude. To make the Fresnel detection independent of the power attenuation caused by distance, we set the mean signal amplitude to 1 and make the signal amplitude always greater than zero.
- We then detect the signal arrival by finding the maximum slope sequence in a PDP to capture the switch in energy from noise to a signal. This achieves a better



(a) Signal propagation when the target is the same distance to the transmitter and receiver. (b) PDP measurements when the distance of the transmitter and receiver is 12 m. (c) PDP measurements when a target is present at different locations.

Fig. 13: Illustration of directed Fresnel signature identification

performance when the signal power is insufficient under a rich-multipath effect occurring aboard a ship.

- Finally, we add a PDP sample with the maximum slope and its following sample for the envelope distribution feature extraction. These two PDP samples are chosen because the uncertain time lag of the WiFi devices will result in the delayed power next to the first signal also containing the LoS path. Two samples are shown in Fig. 12.

Based on a set of normalized and filtered PDP samples from N packets, the Rician- K factor K can be calculated according to Equation 10. The DiFS system is used to continuously monitor the CSI and calculate the K -factor that can indicate the appearance of a human object within the Fresnel zone. For the Rician- K factor, we formulated as a statistical hypothesis test using a pre-calibrated threshold for each of the feature metrics. The hypothesis test is as follows:

$$\begin{cases} H_0 : K \geq \sigma, \\ H_1 : K < \sigma, \end{cases} \quad (11)$$

where H_0 represents the absence of the target and H_1 represents the presence of the target within the Fresnel zone. The threshold σ is the corresponding detection threshold for the Rician- K factor and is calculated according to the reference ship environment measurements.

C. Directed Fresnel Identification

To overcome the undirected Fresnel signature problem described in Section III-C.1, in this section, we propose a fading model-based Fresnel direction estimator by leveraging the skin effect within a metal ship environment.

Claim3: *The Fresnel direction identification, which is impossible for a general environment, can be realized onboard a ship using a metal skin effect.*

As previously described, a directed Fresnel signature is nearly impossible in a symmetrical environment. However, we can achieve a Fresnel direction identification in a ship environment by identifying the skin waves caused by the metal surface of the ship. The rationale of this is shown in Fig. 13a. As can be seen, owing to the skin effect of the signal propagation onboard a ship, the location of a person may lead

to a different shadowing of the propagated signals. To be more specific, the closer people are to the transmitter in the Fresnel zone, the more waves transmitted from the ship's metal surface brought about by the skin effect that will arrive at the receiver. Therefore, we can identify the *Fresnel direction*, i.e., determine the location relationship with transmitters, by quantifying the number of transmitted waves, which herein we call *skin waves*, received by the receiver. Luckily, based on our experiments, the skin waves can be distinguished through a PDP analysis.

To illustrate this observation, two PDP examples from two scenarios, i.e., a target close to the TX and a target close to the RX in a symmetrical corridor, are collected, as shown in Fig. 13b. As can be seen, the powers of the first and second arriving signal paths are similar for two cases, whereas the fourth and fifth are dramatically different. The average difference in the power level of these two delayed times can be nearly 6.05 dB in this symmetrical space, where no other influencing factors remain. Based on this analysis, the delayed power difference can be considered owing to the unique skin effect in such a metal environment. The results in Fig. 13c also show that this effect can be used to break the symmetry problem. To precisely recognize the skin paths, we utilize a power fading model to characterize the multiple paths under the applied scenario and propose an optimization-based algorithm to estimate the distance of each path.

According to wireless communication theory, the power received at the receiver is mainly related to the propagation fading, absorption, and shadow fading. We then model these four types of fading as follows:

- Propagation fading:* According to the Friis model [23], the power attenuation of radio propagation in air can be described as $L(d_{LoS})$ when using the distance d_{LoS} between the transmitters and receivers and the wavelength λ in dBm:

$$L(d_{LoS}) = 10\log[\lambda^2/(16\pi^2 d_{LoS}^2)] \quad (12)$$

- Reflection absorption:* Differing from the LoS path, the NLoS path suffers from multiple reflections and absorptions on the surface. Supposing that there are K reflection paths during propagation, and that the k -th paths can be denoted as follows:

$$R(d_k) = \frac{\gamma_k P_t G_t G_r \lambda^2}{16\pi^2 d_k^2} \quad (13)$$

where γ_k is the reflection coefficient of the k -th path and represents the radio power absorptions.

- *Skin waves attenuation:* Because the conductivity, texture, and dielectric properties of the reflection surface are diverse, a log-normal shadowing model is typically used to characterize this attenuation ψ in decibels.

$$p(\psi) = \frac{10}{\ln 10 \sqrt{2\pi} \sigma_{\psi_{dB}} \psi} \exp \left[-\frac{(10 \ln \psi - \mu_{\psi_{dB}})^2}{2\sigma_{\psi_{dB}}^2} \right] \quad (14)$$

where $\mu_{\psi_{dB}}$ is the mean of $\psi_{dB} = 10 \log_{10} \psi$ and $\sigma_{\psi_{dB}}^2$ is the standard variation.

- *Target absorption:* A WiFi signal experiences random variations owing to a blockage from the localization target. However, the height, size, and location of the target will differ in reality. Because the targets that cause an attenuation are generally random and unknown, herein we denote the target absorption as L_T .

Suppose there are K radio propagation paths between the transmitter and receiver. We combine these models and obtain the NLoS-path received power with parameters d_k , k , and γ_k as follows:

$$P_\psi(d) = L(d_{LoS}) + \sum_k^K R(d_k, \gamma_k) + \psi + L_T \quad (15)$$

The output power level is from -25 to 10 dBm. For a different delay time, we have a different received power $\{|p(t)|, t \in (1, T)\}$. Therefore, we can combine a power model with PDP measurements and develop the following equation:

$$\left\{ \begin{array}{l} \varepsilon_1 = P_\psi(d_1, \gamma_1) - |p(1)| \\ \varepsilon_2 = P_\psi(d_2, \gamma_2) - |p(2)| \\ \dots \\ \varepsilon_K = P_\psi(d_K, \gamma_K) - |p(T)| \end{array} \right. \quad (16)$$

where $d_k = d_1 + C \cdot \Delta t \cdot (k - 1)$, C is the speed of light, and Δt is the time interval of two paths. Here, $\gamma_k = (\gamma_1)^k$ is the approximate reflection attenuation for each path. We then define the total fitting error as follows:

$$\min Loss = \sum_k^K (\|\varepsilon_k\|_2) \quad (17)$$

This optimization problem can be solved using the Newton or Gradient decent method to obtain a numerical result. Our goal is to find the estimated (d_1, d_2, \dots, d_K) for each path by minimizing the total error. We define the skin path as the propagation distance $3d_1 < d_k < 5d_1$ based on our experiments conducted aboard actual ships. We can therefore identify and extract the skin waves. Based on these paths, the skewness of these signal powers, which is a general metric depicting the skewness of the distribution, is used to determine the direction. Mathematically, the skewness s is defined as follows:

$$s = \frac{E\{x - u\}^3}{\sigma^3} \quad (18)$$

Algorithm 2 Construction of directed Fresnel signature table.

Input: 1) Location coordinates of WiFi APs, $TX = \{(ax_i, ay_i) | i \in (1, M)\}$. 2) Location coordinates of WiFi receivers, $RX = \{(bx_i, by_i) | i \in (1, N)\}$. 3) Location matrix of the localization space S .

Output: Localization Signature Table.

▷ Obtain location signature

- 1: $E = \{e_i | i \in (0, M \times N)\} \leftarrow \text{ELLIPSOIDAL}(TX, RX)$
- 2: $SZ \leftarrow \text{GETSUBZONES}(E, S)$
- 3: **for** $i = 0 \leftarrow |SZ|$ **do**
- 4: $\text{Centroid}[i] \leftarrow \text{GETCENTRIOD}(SZ[i])$
- 5: $\text{Signature}[i] \leftarrow \text{GETSIGNATURE}(\text{Centroid}[i])$
- 6: **end for**
- ▷ Obtain directed signature
- 7: $B = \{l_i | i \in (0, M \times N)\} \leftarrow \text{BISECTORLINES}(TX, RX)$
- 8: **for** $i = 0 \leftarrow |SZ|$ **do**
- 9: $\text{DirSignature}[i] \leftarrow \text{GETDIRECTION}(\text{Centroid}[i], B)$
- 10: **end for**
- ▷ Return directed Fresnel signature table
- 11: **return** $\{\text{DirSignature}, \text{Centroid}\}$.

where x , μ , and σ denote the measurement, mean, and standard deviation, respectively. A positive (negative) skewness indicates that the measured data spreads out more toward the right (left) of the sample mean and in a direction toward the transmitter or receiver.

D. Localization of DiFS

DiFS determines the location of the target in a passive way by matching the directed Fresnel signature recognition with all Fresnel signatures. Therefore, a pre-built Fresnel signature table needs to be established prior to the system runtime for a real-time signature search and match. In this section, we propose the use of a *Fresnel signature table* construction algorithm and a signature search method to efficiently realize the DiFS. In addition, we expand the DiFS to multiple target localizations. The procedure of the DiFS localization contains three steps:

- 1) During the offline phase, all subzones are found and their corresponding directed Fresnel signatures are determined in the localization space based on the WiFi AP locations. They are then listed and a *Fresnel signature table* is constructed.
- 2) During the online phase, the CSI of all WiFi links is measured and the Fresnel signature of the current space is determined using our proposed PDP-based detection method. Meanwhile, the signature may be corrupt owing to hardware problems or environmental noise.
- 3) A search of the *Fresnel signature table* is conducted to find the signature most similar to the current measurements, and the centroid of the subzone is assigned to the estimated location of the target.

The pseudocode for constructing the location *Fresnel signature table* is described in Algorithm 2. The descriptions of

each function are as follows:

- ELLIPSOIDAL takes in the locations of the M transmitters and N receivers as input and returns the set $M \times N$ of all pairwise Fresnel ellipsoidal boundaries E within the localization space.
- GETSUBZONES takes in the Fresnel ellipsoidal set E and the localization space S as input and returns subzone sets SZ . Each set includes all locations in space S that are within the subzone. Please refer to [29] Section 8 for a detailed description.
- GETCENTROID takes in locations of subzone set $SZ[i]$ as the input and returns the centroid of all locations given by the following:

$$(cx_i, cy_i) \leftarrow \left(\frac{\sum_j^{SZ[i]} x_j}{|SZ[i]|}, \frac{\sum_j^{SZ[i]} y_j}{|SZ[i]|} \right) \quad (19)$$

- GETSIGNATURE takes in the coordinates of the location and returns the Fresnel signature for that location with respect to the Fresnel ellipsoidal boundary sets.
- BISECTORLINES takes in the locations of M transmitters and N receivers as input and returns the set $M \times N$ of all pairwise perpendicular bisector lines B .
- GETDIRECTION takes in the coordinates of the location and the perpendicular bisector lines B to determine the Fresnel direction for that location.

Next, we present a metric used to measure the distance between two signatures. The Spearman's rank order correlation coefficient [30], which is a metric used to rank the orders, is chosen to capture the similarity of two signatures. Given two sequence vectors $S_1 = \{u_i\}$ and $S_2 = \{v_i\}$, $1 \leq i \leq n$, the metric is defined as the linear correlation coefficient of the elements as follows:

$$\rho = 1 - \frac{6 \sum_{i=1}^n (u_i - v_i)^2}{n(n^2 - 1)}. \quad (20)$$

Theorem 2. *The proposed signature search method takes $O(n^3 \log(n))$ as the worst case time, and $O(n^3)$ as the worst case space to search the location sequence.*

Proof: The functions GETSUBZONES and BISECTORLINES take $O(n^2)$ time and space, respectively. Calculating the Spearman's coefficient of the newly measured signature with the existing signature table costs $O(n \log n)$ operations and $O(n)$ in space. Because the location sequence table is of size $O(n^2)$, searching through it takes a time of $O(n^3 \log n)$ and space of $O(n^3)$.

Multi-target localization. We further extend our system to the multi-target localization. The *intuition* here is that each separated target can be detected individually by measuring a subset of non-overlapping WiFi Fresnel zones. When the targets are located sparsely and the Fresnel zones are not overlapped, one target can only affect one wireless link. We can estimate the number of targets and their approximate locations accordingly. The pseudocode for constructing such a *multi-target Fresnel signature* is shown in Algorithm 3. Next, based on our proposed Fresnel detection method, we can then identify the blocked links and estimate the number of targets and their location according to the Fresnel signature

Algorithm 3 Construction of multi-target Fresnel signature table.

Input: 1) Location coordinates of $TX = \{(ax_i, ay_i) | i \in (1, M)\}$, and $RX = \{(bx_i, by_i) | i \in (1, N)\}$.
Output: Multi-target signature table.
 ▷ Calculate the overlapping number of links
1: $E = \{e_i | i \in (0, M \times N)\} \leftarrow \text{ELLIPSOIDAL}(TX, RX)$
2: $W \leftarrow \text{OVERLAPCOUNT}(E)$
 ▷ Sort sequence E in ascending order of W
3: $(E, W) \leftarrow \text{SORT}(E, W)$
 ▷ Select link set V from E
4: $V[0] \leftarrow E[0]$
5: **for** $i = 1 \leftarrow |E|$ **do**
6: **if** $\text{OVERLAP}(V, E[i]) = \text{False}$ **then** $V \leftarrow E[i]$
7: **end if**
8: **end for**
 ▷ Return the Fresnel signature table
9: $C \leftarrow \text{GETCENTROID}(V)$
10: **return** $\{V, C\}$.

table. However, when numerous targets exist or two targets are extremely close to each other, it remains challenging to accurately localize both of them.

V. IMPLEMENTATION AND EXPERIMENT

In this section, we introduce the framework of the DiFS system and its modules, including the controller, localizer, history, and database. The performance was also evaluated under different environments.

A. Experimental testbed

To verify the performance of the DiFS system, we conducted experiments aboard an actual passenger ship, dubbed China Goddess 2 Cruise. We deployed our experimental testbed under two scenarios, i.e., in a multi-function hall and a dining room, the sizes of which are $7.5m \times 13.5m$ and $15m \times 20m$, respectively. Among them, the hall is the biggest room in the ship with little furniture or few obstacles with strong LoS paths. By contrast, a bar is full of tables and a counter, which generate rich NLoS paths. The floorplan of the testing deck and device deployment are shown in Fig. 14.

B. Hardware and Software

The hardware of the DiFS system consists of four components: WiFi devices, including all IoT tags with WiFi modules, CSI collectors, a background server, and a foreground PC. In our implementation, the CSI collectors are Thinkpad T-serial laptops with an Intel 5300 wireless NIC installed, each equipped with three external antennas, with each having 4G memory and running Ubuntu 14.04 LTS. The WiFi APs are TP-LINK routers, operating within the 2.4 GHz band with a bandwidth of 20 MHz. In the system, the collectors are configured to receive packets in monitor mode and extract the CSI data using open-source CSI tools. The CSI data are then passed to the background server through the TCP/IP protocol.

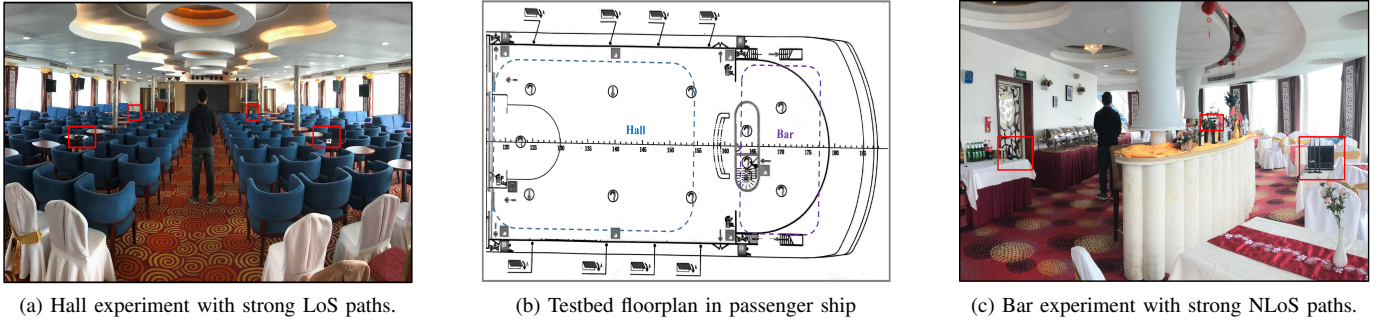


Fig. 14: Experimental environment and device deployment.

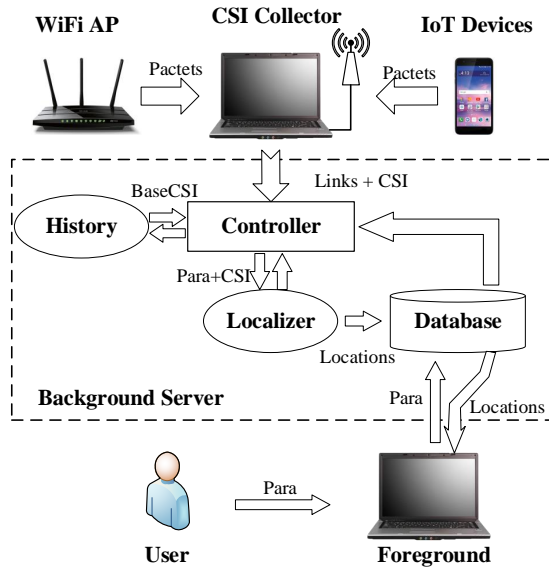


Fig. 15: System framework of DiFS.

A system service program is set up on this server using a 3.40 GHz Intel E3-1231 CPU and 16 GB of RAM. A foreground PC is used to run the software and show the locations in real-time. The framework is shown in Fig. 15. There are three kernel parts in the background server:

- **Controller:** The controller is the kernel of the DiFS system and controls the main flows using the algorithm introduced above. The localizer and database operate according to its commands.
- **Database:** The database is used to store the data including real-time and historical locations. During the run-time phase, the database stores the parameters, including the WiFi AP locations, baseline CSI, and characteristics of the scenario.
- **Localizer:** The localizer is used to initialize the space map after receiving the parameters from the users and compute the Fresnel signature table using Algorithm 2. Then, after receiving the online CSI measurements from the controller, the results are compared with the previous records to identify the number of targets. Finally, the localizer checks and fits the directed Fresnel signature table and returns the estimated coordinates of the target.

C. Deployment setup

In this experiment, we set three APs at a height of 1.2 m above the ground and two CSI collectors on a table also with a height of 1.2 m. The Fresnel zone parameters can be calculated according to Equation 4. Herein, we set $n = 3$ for the third Fresnel zone, which is suitable for a map segmentation and the Fresnel detection. To create the communication links, the CSI collectors continuously ping the APs at a frequency of 10 packets per second (pkts). Unless specifically mentioned, in the remainder of this paper, we refer to the default setup introduced herein for a performance evaluation.

D. Evaluation Criterion

Before the evaluation, we propose the evaluation criterion of localization. A real-time error is calculated as the minimum distance between the centroid of the estimated location subzone and this true location, as shown in Eq. 21.

$$Error(t) = \sqrt{(\hat{x} - X_g)^2 + (\hat{y} - Y_g)^2} \quad (21)$$

in which \hat{x}, \hat{y} are the estimated location coordinates, and X_g, Y_g are the ground-truth location coordinates. To evaluate the system performance of the entire process, we also define an accumulated error as follows:

$$AccuError(t) = \int_0^t Error(t) \quad (22)$$

In addition, because most human targets have a width of narrower than 0.5 m, we regard a target estimation of within 0.5 cm as an accurate localization result.

E. Overall Localization Accuracy

In this section, the DiFS system is compared with four state-of-the-art techniques in the indoor environment of an actual passenger ship, which are described as follows:

- **Pilot** uses the CSI correlations of all subcarriers as fingerprints, and the kernel density-based maximum a posteriori probability algorithm to localize a target.
- **LiFS** is a passive state-of-the-art target localization method that utilizes the power fading model to estimate the target locations.
- **FiDo** is an approach to fine-grained WiFi-based localization designed to cater to unlabelled users. It employs

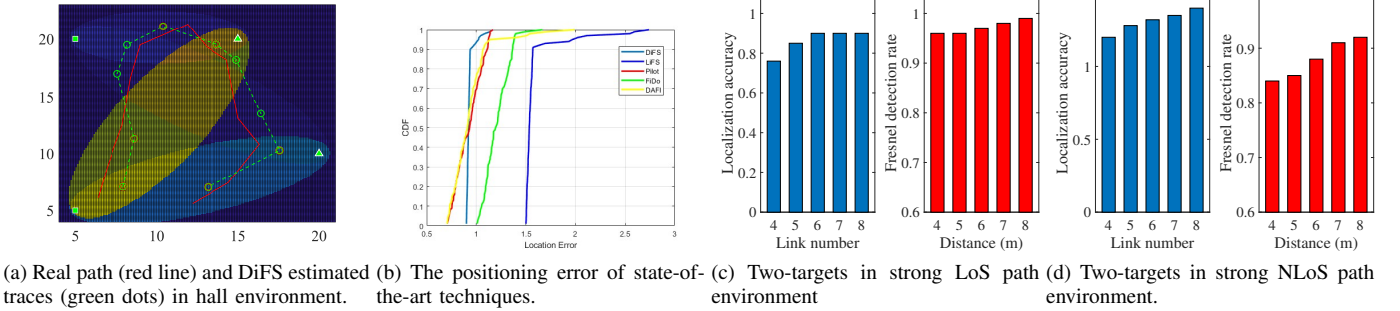


Fig. 16: DiFS Performance in ship environment.

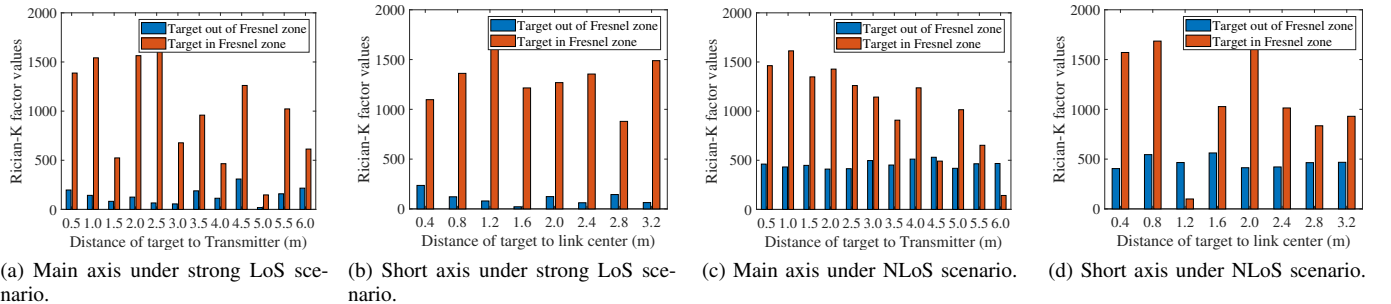


Fig. 17: Fresnel detection accuracy under LoS and NLoS scenarios.

domain adaptation techniques to refine, adjust, and improve location estimations for enhanced accuracy and ubiquity, particularly when static environmental changes occur. [31]

- **DAFI** is an innovative method for device-free indoor localization based on WiFi signals. It leverages domain adaptation techniques to enhance location accuracy and versatility for tracking objects or individuals without the need for specialized devices, mitigating the impact of environmental changes. [32]

The test datasets were collected during two ship voyages. During the experiment, we employed five volunteers, both male and female, as localized targets and estimated their locations using the CSI data in each room. The volunteers were set to repeatedly change their posture into sitting and standing positions. During a 5-day voyage, the cruise ship stopped twice at different ports each day. Therefore, we were able to test these methods for ten rounds under both sailing and anchored conditions. To objectively evaluate the accuracy in a mobile ship environment, we randomly chose ten different times during the voyage during both the day and night.

The overall experiment error results are shown in Table. II. Among them, FiDo and LiFS are significantly impacted by the environmental characteristics of the ship, resulting in a notable decrease in accuracy when the ship is in motion. While DAFI and Pilot may occasionally exhibit lower positioning errors compared to DiFS, in most cases, their positioning errors are considerably higher than those of DiFS, especially when ships encounter rough seas. These two methods cannot ensure reliable stability. By contrast, the DiFS performs well onboard

TABLE II: Comparison of the results among the four methods used onboard a ship.

System	Accuracy in Ship	Weakness
Pilot	0.7-1.2 m	Need intensive site survey
LiFS	1.5-2.7 m	Complex power model in ship
FiDo	1.0-1.6 m	Need intensive site survey
DAFI	0.7-2 m	Extensive preliminary work
DIFS	0.9-1.2 m	Challenge in multiple targets

a ship. In Fig. 16a, the DiFS can accurately estimate the subzone of the target and track the path in a precise manner. The experiment results in general office and ship environments are also shown in Fig. 16b. It was concluded that the DiFS can achieve a better performance with a higher robustness and less complexity for a dynamic ship environment. We also evaluated **two-target localization** with the increasing impact of the links on the DiFS system. Increasing the communication links from 4 to 8, as shown in Figs. 16c and 16d, the left subgraph demonstrates the accuracy with the link number and the right subgraph depicts the Fresnel detection rate with distance between a pair of transmitters. The figures demonstrate that, although the detection rate is decreased when the distance of the transmitters decrease, the accuracy of the detection is over 90% and the localization accuracy can increase owing to a finer grid map segmentation.

F. Fresnel Detection Accuracy

In this section, we discuss the accuracy of the PDP-based Fresnel target detection as the most important criteria of the

DiFS system. We evaluated it under two different environments, i.e., an open hall (with a strong LoS) and a bar (with a strong NLoS) onboard a ship, as shown in Fig. 14. The results are shown in Fig. 17.

1) Evaluation under LoS scenarios: In Fig. 17a, the K-factor values of the target at each distance from the transmitter to the receiver (major axis of the ellipse) are shown. As can be seen, in over 82% of the cases, the K-factor can accurately reflect the location. We also show the target distance to the link center (along the short axis) in Fig. 17b. The Fresnel detection accuracy is over 87%. Therefore, it can be concluded that under a strong LoS scenario, our proposed PDP-based target detection method performs well.

2) Evaluation under NLoS scenarios: We chose a bar environment to evaluate the localization errors for the DiFS. The median error is 1.6-times higher under the NLoS scenario than under the LoS scenario. The decrease in accuracy of the DiFS under the NLoS scenario is mainly due to the blocking of the bar counter, which can significantly reduce the signal power of the LoS path identified by the DiFS. As shown in Figs. 17c and 17d, when all targets are located in the bar, the mean K-factor can also be used to detect the target, although with a slight decrease in accuracy. Fig. 16d also shows that the detection accuracy can remain at more than 85% if the distance between each transmitter is less than 8 m. This implies that the DiFS system can also perform well in the NLoS if the AP locations are set well.

G. Efficiency and Scalability.

Because the system was designed to achieve energy efficiency, the DiFS uses only beacons from the APs in a single channel. It synchronizes with the beacon-schedules of these APs and periodically wakes up to collect the CSIs. Moreover, because it is more energy efficient to launch a system service than an application, the consumption can be further reduced. To this end, according to our evaluation, maintaining a background data collection application leads to an additional power consumption of only approximately 10%, which is affordable for most mobile COTS devices.

VI. CONCLUSION

In this study, we designed and implemented one of the first fingerprint-free WiFi-based passive human localization systems developed for a dynamic ship environment. Compared with other passive localization methods, the proposed DiFS does not require any explicit pre-deployment effort and can overcome the significant effects of a deployment within a mobile ship environment. Real-world implementation and evaluation results show that the appropriate deployment method according to the static environment can ensure that the transceiver can maintain a good positioning effect when the transceiver communicates in the LoS environment.

ACKNOWLEDGMENT

This work was supported by the National Natural Science Foundation of China (NSFC) under Grant No. 51979216 , Natural Science Foundation of Hubei Province , China, under

Grant No. 2021CFA001 and Natural Science Foundation of Hubei Province Youth Program under Grant No. 20221J0059.

REFERENCES

- [1] Y. Shu, K. G. Shin, T. He, and J. Chen, "Last-mile navigation using smartphones," in *Proceedings of the 21st Annual International Conference on Mobile Computing and Networking*. ACM, 2015, pp. 512–524.
- [2] C.-W. Chu, H.-A. Lu, and C.-Z. Pan, "Emergency evacuation route for the passenger ship," *Journal of Marine Science and Technology*, vol. 21, no. 5, pp. 515–521, 2013.
- [3] J. Wang, H. Jiang, J. Xiong, K. Jamieson, X. Chen, D. Fang, and B. Xie, "LiFS," *Proceedings of the 22nd Annual International Conference on Mobile Computing and Networking - MobiCom '16*, pp. 243–256, 2016. [Online]. Available: <http://dl.acm.org/citation.cfm?doid=2973750.2973776>
- [4] T. Kim, S. Nazir, and K. I. Overgard, "A stamp-based causal analysis of the korean sewol ferry accident," *Safety Science*, vol. 83, pp. 93–101, 2016.
- [5] K. Qian, C. Wu, Y. Zhang, G. Zhang, Z. Yang, and Y. Liu, "Widar2 . 0 : Passive Human Tracking with a Single Wi-Fi Link," *ACM International Conference on Mobile Systems, Applications, and Services (MobiSys)*, 2018.
- [6] X. Li, S. Li, D. Zhang, J. Xiong, Y. Wang, and H. Mei, "Dynamic-music: accurate device-free indoor localization," in *Proceedings of the 2016 ACM International Joint Conference on Pervasive and Ubiquitous Computing*. ACM, 2016, pp. 196–207.
- [7] J. Xiao, K. Wu, Y. Yi, L. Wang, and L. M. Ni, "Pilot: Passive Device-Free Indoor Localization Using Channel State Information," *2013 IEEE 33rd International Conference on Distributed Computing Systems*, pp. 236–245, 2013. [Online]. Available: <http://ieeexplore.ieee.org/document/6681593/>
- [8] W. Wang, A. X. Liu, M. Shahzad, K. Ling, and S. Lu, "Understanding and Modeling of WiFi Signal Based Human Activity Recognition," *Proceedings of the 21st Annual International Conference on Mobile Computing and Networking - MobiCom '15*, pp. 65–76, 2015. [Online]. Available: <http://dl.acm.org/citation.cfm?doid=2789168.2790093>
- [9] Q. Pu, K.-Y. Ng, Joseph, and M. Zhou, "Fingerprint-based localization performance analysis: From the perspectives of signal measurement and positioning algorithm," *IEEE Internet of Things Journal*, vol. 70, 2021.
- [10] X. Wang, L. Gao, S. Mao, and S. Pandey, "Deepfi: Deep learning for indoor fingerprinting using channel state information," in *2015 IEEE wireless communications and networking conference (WCNC)*. IEEE, 2015, pp. 1666–1671.
- [11] M. Chen, K. Liu, J. Ma, and C. Liu, "Spatio-temporal fingerprint localization for shipboard wireless sensor networks," *IEEE Sensors Journal*, vol. 18, no. 24, pp. 10 125–10 133, 2018.
- [12] K. Liu, M. Chen, E. Cai, J. Ma, and S. Liu, "Indoor localization strategy based on fault-tolerant area division for shipboard surveillance," *Automation in Construction*, vol. 95, pp. 206–218, 2018.
- [13] G. W. Jiang, S. H. Fu, Z. C. Chao, and Q. F. Yu, "Pose-relay videometrics based ship deformation measurement system and sea trials," *Chinese Science Bulletin*, vol. 56, no. 1, pp. 113–118, 2011.
- [14] A. V. Mochalov and O. Jo, "Use of the ring laser units for measurement of the moving object deformations," *Second International Conference on Lasers for Measurements and Information Trans. SPIE*, vol. 4680, no. February 2002, pp. 85–92, 2002.
- [15] D. Wu, D. Zhang, C. Xu, Y. Wang, and H. Wang, "WiDir: walking direction estimation using wireless signals," *Proceedings of the 2016 ACM International Joint Conference on Pervasive and Ubiquitous Computing - UbiComp '16*, pp. 351–362, 2016. [Online]. Available: <http://dl.acm.org/citation.cfm?doid=2971648.2971658>
- [16] T. Öktem and D. Slock, "Power delay Doppler profile fingerprinting for mobile localization in NLOS," *IEEE International Symposium on Personal, Indoor and Mobile Radio Communications, PIMRC*, pp. 876–881, 2010.
- [17] D. Mattis and J. Bardeen, "Theory of the anomalous skin effect in normal and superconducting metals," *Physical Review*, vol. 111, no. 2, p. 412, 1958.
- [18] K. Liu, Z. Tian, Z. Li, and M. Zhou, "Rfloc: A reflector-assisted indoor localization system using a single-antenna ap," *IEEE Transactions on Instrumentation and Measurement*, vol. 70, 2021.
- [19] M. Chen, K. Liu, J. Ma, Y. Gu, Z. Dong, and C. Liu, "Swim: Speed-aware wifi-based passive indoor localization for mobile ship environment," *IEEE Transactions on Mobile Computing*, vol. 20, no. 2, pp. 765–779, 2019.

- [20] M. Chen, K. Liu, J. Ma, X. Zeng, Z. Dong, G. Tong, and C. Liu, "Moloc: Unsupervised fingerprint roaming for device-free indoor localization in a mobile ship environment," *IEEE Internet of Things Journal*, 2020.
- [21] M. Kotaru, K. Joshi, D. Bharadia, and S. Katti, "SpotFi : Decimeter Level Localization Using WiFi," *Sigcomm 2015*, pp. 269–282, 2015. [Online]. Available: Stanford University
- [22] X. Chen, C. Ma, M. Allegue, and X. Liu, "Taming the inconsistency of Wi-Fi fingerprints for device-free passive indoor localization," *Proceedings - IEEE INFOCOM*, 2017.
- [23] X. Guo, D. Zhang, K. Wu, and L. M. Ni, "MODLoc: Localizing multiple objects in dynamic indoor environment," *IEEE Transactions on Parallel and Distributed Systems*, vol. 25, no. 11, pp. 2969–2980, 2014.
- [24] D. Tse and P. Viswanath, *Fundamentals of wireless communication*. Cambridge university press, 2005.
- [25] D. Halperin, W. Hu, A. Sheth, and D. Wetherall, "Predictable 802.11 packet delivery from wireless channel measurements," *ACM SIGCOMM Computer Communication Review*, vol. 40, p. 159, 2010.
- [26] Y. Xie, Z. Li, and M. Li, "Precise Power Delay Profiling with Commodity WiFi," *Proceedings of the 21st Annual International Conference on Mobile Computing and Networking - MobiCom '15*, pp. 53–64, 2015. [Online]. Available: <http://dl.acm.org/citation.cfm?doid=2789168.2790124>
- [27] J. Wang, J. Xiong, H. Jiang, K. Jamieson, X. Chen, D. Fang, and C. Wang, "Low Human-Effort, Device-Free Localization with Fine-Grained Subcarrier Information," *IEEE Transactions on Mobile Computing*, vol. 1233, no. c, pp. 1–14, 2018.
- [28] Z. Zhou, Z. Yang, C. Wu, W. Sun, and Y. Liu, "LiFi: Line-Of-Sight identification with WiFi," *Proceedings - IEEE INFOCOM*, pp. 2688–2696, 2014.
- [29] M. Van Kreveld, O. Schwarzkopf, M. de Berg, and M. Overmars, *Computational geometry algorithms and applications*. Springer, 2000.
- [30] B. P. Flannery, S. A. Teukolsky, W. H. Press, and W. T. Vetterling, *Numerical recipes in C: The art of scientific computing*. Cambridge university press, 1988, vol. 2.
- [31] X. Chen, H. Li, C. Zhou, X. Liu, D. Wu, and G. Dudek, "Fido: Ubiquitous fine-grained wifi-based localization for unlabelled users via domain adaptation," *Proceedings of The Web Conference*, pp. 23–33, 2020.
- [32] L. Hang, C. Xi, W. Ju, W. Di, and L. Xue, "Dafi: Wifi-based device-free indoor localization via domain adaptation," *Proceedings of the ACM on Interactive, Mobile, Wearable and Ubiquitous Technologies*, vol. 5, no. 4, pp. 1–21, 2021.



Cong Chen used to be the general manager of the R&D center of Tianhai Fusion Defense Equipment Technology Co., Ltd., focusing on the design of passenger ships, luxury cruise ships, LNG-powered ships, and bulk cargo ships. The first 500-passenger luxury tourist ship in China won the National Tourism Administration And the authoritative recognition of Weihai Municipal Government.



Xyming Zeng received the Ph.D. degree in the Geodetection and Information Technology from the China University of Geosciences, China, in 2018. He is currently working toward the Postdoctoral with the Traffic and Transportation Engineering, School of Navigation, Wuhan University of Technology, China. From 2016 to 2017, he was a joint training Ph.D. student with Electrical and Computer Engineering, Florida State University, Tallahassee, FL, USA. His research interests include routing protocols, and performance analysis, for wireless networks.



Guangmo Tong is an Assistant Professor in the Department of Computer and Information Sciences at the University of Delaware. He received a Ph.D. in Computer Science at the University of Texas at Dallas in 2018. He received his BS degree in Mathematics and Applied Mathematics from Beijing Institute of Technology in July 2013. His research interests include computational social systems, machine learning, and theoretical computer science.



Kezhong Liu received the B.S. and M.S. degrees in marine navigation from the Wuhan University of Technology(WUT), Wuhan, China, in 1998 and 2001, respectively. He received the Ph.D. degree in communication and information engineering from the Huazhong University of Science and Techonogy, Wuhan, China, in 2006. He is currently a professor with School of Navigation, WUT. His active research interests include indoor localization technology and data mining for ship navigation.



Mozi Chen received the B.S. degree in electric engineering from the Hubei University of Technology, China, in 2013, and the M.S. degree in navigation engineering from the Wuhan University of Technology (WUT), China, in 2016. He is currently a Ph.D. student in WUT. His research work has been focusing on wireless sensing techniques and machine learning algorithms for human localization, emergency navigation and activity recognition in mobile environment, i.e., cruise ships.



Guoyu Wang received the B.S. degree in electric engineering from the Wuhan University of Technology (WUT), China, in 2016, and the M.S. degree in navigation engineering from WUT, China, in 2019. He is currently a Ph.D. student in WUT. He research interests focus on wireless localization and none line of sight indoor localization.